*Inorg. Chem.* **2005**, *44*, 9731–9742


# Inorganic–Metalorganic Hybrids Based on Copper(II)-Monosubstituted Keggin Polyanions and Dinuclear Copper(II)–Oxalate Complexes. Synthesis, X-ray Structural Characterization, and Magnetic Properties

**Santiago Reinoso,[†] Pablo Vitoria,[†] Juan M. Gutiérrez-Zorrilla,*[,†] Luis Lezama,*[,†] Leire San Felices,[†] and Javier I. Beitia[‡]**

*Departamento de Química Inorgánica, Facultad de Ciencia y Tecnología, Universidad del País Vasco, Apartado 644, E-48080 Bilbao, Spain, and Departamento de Química Inorgánica, Facultad de Farmacia, Universidad del País Vasco, Apartado 450, E-01080 Vitoria, Spain*

Received July 8, 2005

Reaction of in situ generated copper(II)-monosubstituted Keggin polyoxometalates and copper(II)–bipyridine–oxalate complexes in the corresponding alkaline acetate buffer led to the formation of hybrid metal organic–inorganic compounds $K_2[\{SiW_{11}O_{39}Cu(H_2O)\}\{Cu_2(bpy)_2(H_2O)_2(\mu\text{-ox})\}_2]\cdot 14H_2O$ (**1**), $K_{14}[\{SiW_{11}O_{39}Cu(H_2O)\}\{Cu_2(bpy)_2(\mu\text{-ox})\}]_2[SiW_{11}O_{39}Cu(H_2O)]\cdot 55H_2O$ (**2**), $(NH_4)_4[\{SiW_{11}O_{39}Cu(H_2O)\}\{Cu_2(bpy)_2(\mu\text{-ox})\}]\cdot 10H_2O$ (**3**), and $Rb_4[\{SiW_{11}O_{39}Cu(H_2O)\}\{Cu_2(bpy)_2(\mu\text{-ox})\}]\cdot 10H_2O$ (**4**). Their structures have been established by single-crystal X-ray diffraction. The main structural feature of these compounds is the presence of copper(II)-monosubstituted α-Keggin polyoxoanions as inorganic building blocks, on which the $\mu$-oxalatodicopper metalorganic blocks are supported. Compound **1** contains the discrete hybrid polyanion $[\{SiW_{11}O_{39}Cu(H_2O)\}\{Cu_2(bpy)_2(H_2O)_2(\mu\text{-ox})\}_2]^{2-}$, whereas the polymeric hybrid polyanion $[\{SiW_{11}O_{39}Cu(H_2O)\}\{Cu_2(bpy)_2(\mu\text{-ox})\}_2]_n^{4n-}$ gives a monodimensional character to compounds **2**–**4**. Magnetic and EPR results are discussed with respect to the crystal structure of the compounds. DFT calculations on both the $[Cu_2(bpy)_2(H_2O)_4(\mu\text{-ox})]^{2+}$ cationic complex and the metalorganic blocks have been performed in order to determine the optimized geometry and the magnetic coupling constants, respectively.

## Introduction

Polyoxometalates[1] (POMs) constitute a large family of compounds of surprising electronic versatility and structural diversity, which endow them with applications in fields such as catalysis,[2] material science,[3] medicine,[4] and photochemistry.[5] There are already more commercial applications of polyoxometalates than any other class of cluster compounds.[6]

It has long been recognized that the ability to functionalize polyoxometalate anions would extend their versatility and

* To whom correspondence should be addressed. E-mail: juanma.zorrilla@ehu.es (J.M.G.-Z.), luis.lezama@ehu.es (L.L.). Fax: +34946013500.

[†] Departamento de Química Inorgánica, Facultad de Ciencia y Tecnología, Universidad del País Vasco.

[‡] Departamento de Química Inorgánica, Facultad de Farmacia, Universidad del País Vasco.

(1) (a) Pope, M. T.; Müller, A. *Angew. Chem., Int. Ed.* **1991**, *30*, 34. (b) Pope, M. T., Müller, A., Eds. *Polyoxometalates: From Platonic Solids to Antiretroviral Activity*; Kluwer: Dordrecht, The Netherlands, 1994. (c) Hill, C. L., Ed. *Chem. Rev.* **1998**, *98*, 1, special thematic issue. (d) Pope, M. T., Müller, A., Eds. *Polyoxometalate Chemistry: From Topology via Self-Assembly to Applications*; Kluwer: Dordrecht, The Netherlands, 2001. (e) Pope, M. T., Yamase, T., Eds. *Polyoxometalate Chemistry for Nanocomposite Design*; Kluwer: Dordrecht, The Netherlands, 2002. (f) Borrás-Almenar, J. J., Coronado, E., Müller, A., Pope, M. T., Eds. *Polyoxometalate Molecular Science*; Kluwer: Dordrecht, The Netherlands, 2003. (g) Pope M. T. In *Comprehensive Coordination Chemistry II*; McCleverty, J. A., Meyer, T. J., Eds.; Elsevier Ltd.: Oxford, U.K., 2004.

(2) (a) Misono, M. *Catal. Rev.—Sci. Eng.* **1988**, *30*, 339. (b) Ilkenhaus, T.; Herzorg, B.; Braun, T.; Schlögl, R. *J. Catal.* **1995**, *153*, 275. (c) Belanger, R.; Moffat, J. B. *J. Catal.* **1995**, *152*, 171. (d) Corma, A. *Chem. Rev.* **1995**, *95*, 559. (e) Hill, C. L.; Prosser-Mccartha, M. *Coord. Chem. Rev.* **1995**, *143*, 407. (f) Kozhevnikov, I. V. *Catal. Rev.—Sci. Eng.* **1995**, *37*, 311. (g) Neumann, R. *Prog. Inorg. Chem.* **1998**, *47*, 317. (h) Okuhara, T.; Mizuno, N.; Misono, M. *Adv. Catal.* **1996**, *41*, 113. (i) Kuznetsova, L. I.; Maksimov, G. M.; Likholobov, V. A. *Kinet. Catal.* **1999**, *40*, 622. (j) Misono, M. *Chem. Commun.* **2001**, 1141. (k) Khenkin, A. M.; Weiner, L.; Wang, Y.; Neumann, R. *J. Am. Chem. Soc.* **2001**, *123*, 8531. (l) Kozhevnikov, I. V. *Catalysts for Fine Chemicals, Vol 2. Catalysis by Polyoxometalates*; Wiley: Chichester, U.K., 2002. (m) Kozhevnikov, I. V. *Innovations Pharm. Technol.* **2003**, *3*, 96. (n) Okun, N. M.; Travis, M.; Hardcastle, K. I.; Hill, C. L. *Inorg. Chem.* **2003**, *42*, 6610. (o) Kiricsi, I., Ed. *Appl. Catal., A* **2003**, *256*, 1, special issue. (p) Hill, C. L. *Angew. Chem., Int. Ed.* **2004**, *43*, 402. (q) Liu, H.; Iglesia, E. *J. Catal.* **2004**, *223*, 161. (r) Stahl, S. S. *Angew. Chem., Int. Ed.* **2004**, *43*, 3400. (s) Kholdeeva, O. A.; Vanina, M. P.; Timofeeva, N. N.; Maksimovskaya, R. I.; Trubitsina, T. A.; Melgunov, M. S.; Burgina, E. B.; Mrowiec-Bialon, J.; Jarzebski, A. B.; Hill, C. L. *J. Catal.* **2004**, *226*, 363. (t) Won, B. K.; Voitl, T.; Rodríguez-Rivera, G. J.; Dumesic, J. A. *Science* **2004**, *305*, 1280.

10.1021/ic051134m CCC: $30.25 
Published on Web 12/01/2005

lead to new and more selective applications. The chemistry of POM-based hybrids has been significantly enriched by the inclusion of transition-metal (TM) coordination complexes into the hybrid system, either to provide charge compensation or as a part of the inorganic POM framework itself.[7] To date, several of these hybrid compounds based on vanadium and molybdenum isopolyanions have been reported; in contrast, the number of examples incorporating Keggin heteropolyanions and their derivatives as the inorganic component is still significantly lower.[8] Given the relevance of precise compositions and structures in all the investigations focused on this class of clusters, the continuing development of synthetic methods for the systematic modification of POM systems remains very important.[9]

Currently, we are interested in exploring the applicability of Keggin POMs and TM−carboxylate cationic complexes in the preparation of new magnetically attractive hybrid compounds.[10] The present paper reports the synthesis, crystal structure, and magnetic properties of a series of salts based on dinuclear copper(II)−oxalate−bipyridine cationic complexes supported on copper(II)-monosubstituted Keggin POMs. The interest in supporting TM−oxalate complexes, which have been extensively studied in magnetostructural research works, on Keggin POMs lies in the possibility of tuning the magnetic properties because of their strong dependence on the nature and spatial disposition of the ligands.[11] Moreover, the dimers could play the role of structure-directing agents, so that the Keggin POMs could be templated to lead to open structures with tailorable pore shapes and sizes.

## Experimental Section

**Materials and Methods.** The $K_8[\alpha\text{-}SiW_{11}O_{39}]$ precursor was synthesized according to the procedure described in the literature.[12] All other chemicals were obtained from commercial sources, and were used without further purification. Infrared spectra for solid samples were obtained as KBr pellets on a Mattson 1000 FT-IR spectrometer. Thermogravimetric analysis (TGA) and differential thermal analysis (DTA) were carried out on a TA Instruments SDT 2960 thermobalance under a 100 mL/min flow of synthetic air; the temperature was ramped from 20 to 800 °C at a rate of 5 °C/min. The magnetic susceptibility was measured on a Quantum Design MPMS-7 SQUID magnetometer (*T* range: 5−300 K; applied field: 0.1 T; diamagnetic corrections estimated from Pascal's constants). EPR powder spectra were recorded on a Bruker ESP300 spectrometer (X- and Q-bands) equipped with Oxford low-temperature devices (magnetic field calibration: NMR probe; determination of the frequency inside the cavity: Hewlett-Packard 5352B microwave frequency counter; maintenance of the crystal structures in the powder samples was confirmed by powder X-ray diffraction; computer simulation: WINEPR-Simfonia, version 1.5, Bruker Analytische Messtechnik GmbH). C, N, and H were determined by organic microanalysis on a LECO CHNS 932 analyzer. Cu and K were determined on a Perkin-Elmer 4110ZL AAS analyzer. Rb was determined on a Termo Elemental X7 ICP-MS analyzer.

**Synthesis of $K_2[\{SiW_{11}O_{39}Cu(H_2O)\}\{Cu_2(bpy)_2(H_2O)_2(\mu\text{-}ox)\}_2]\cdot 14H_2O$ (1).** Both the cationic complex $[\{Cu(bpy)(H_2O)\}_2(\mu\text{-}ox)]^{2+}$ (**A**) and the α-Keggin anion $[SiW_{11}O_{39}Cu(H_2O)]^{6-}$ (**B**) were prepared in situ. For **A**, to an aqueous solution (20 mL) of $CuCl_2\cdot 2H_2O$ (68 mg, 0.4 mmol) were successively added solutions of 2,2′-bipyridine (62 mg, 0.4 mmol) in methanol (10 mL) and


(3) (a) Gómez-García, C. J.; Coronado, E.; Ouahab, L. *Angew. Chem., Int. Ed.* **1992**, *31*, 240. (b) Coronado, E.; Gómez-García, C. J. *Comments Inorg. Chem.* **1995**, *17*, 255. (c) Clemente-Juan, J. M.; Coronado, E. *Coord. Chem. Rev.* **1999**, *193*−*195*, 361. (d) Ouahab, L. *Chem. Mater.* **1997**, *9*, 1909; *Coord. Chem. Rev.* **1998**, *178*−*180*, 1501. (e) Coronado, E.; Galán-Mascarós, J. R.; Giménez-Sáiz, C.; Gómez-García, C. J. *Adv. Mater. Opt. Electron.* **1998**, *8*, 61. (f) Kurth, D. G.; Lehmann, P.; Volmer, D.; Müller, A.; Schwahn, D. *J. Chem. Soc., Dalton Trans.* **2000**, 3989. (g) Clemente-León, M.; Coronado, E.; Delhaes, P.; Gómez-García, C. J.; Mingolaud, C. *Adv. Mater.* **2001**, *13*, 574. (h) Clemente-León, M.; Coronado, E.; Gómez-García, C. J.; Martínez-Ferrero, E. *J. Cluster Sci.* **2002**, *13*, 381. (i) Clemente-Juan, J. M.; Coronado, E.; Forment-Aliaga, A.; Galán-Mascarós, J. R.; Giménez-Sáiz, C.; Gómez-García, C. J. *Inorg. Chem.* **2004**, *43*, 2689. (j) Forment-Aliaga, A.; Coronado, E.; Feliz, M.; Gaita-Ariño, A.; Llusar, R.; Romero, F. M. *Inorg. Chem.* **2004**, *43*, 8019. (k) Casañ-Pastor, N.; Gómez-Romero, P. *Front. Biosci.* **2004**, *9*, 1759. (l) Bassil, B. S.; Nellutla, S.; Kortz, U.; Stowe, A. C.; van Tol, J.; Dalal, N. S.; Keita, B.; Nadjo, L. *Inorg. Chem.* **2005**, *44*, 2659. (m) Mialane, P.; Dolbecq, A.; Marrot, J.; Riviere, E.; Sécheresse, F. *Chem.*−*Eur. J.* **2005**, *11*, 1771. (n) Kortz, U.; Hussain, F.; Reicke, M. *Angew. Chem., Int. Ed.* **2005**, *44*, 2.

(4) (a) Michelon, M.; Hervé, M.; Hervé, G. *Biochim. Biophys. Acta* **1987**, *916*, 402. (b) Yamase, T.; Fujita, M.; Fukushima, K. *Inorg. Chim. Acta* **1988**, *151*, 15. (c) Chottard, G.; Hill, C. L.; Weeks, M. S.; Schinazi, R. F. *J. Med. Chem.* **1990**, *33*, 2767. (d) Inouye, Y.; Tale, Y.; Tokutake, Y.; Yoshida, T.; Yamamoto, A.; Yamase, T.; Nakamura, S. *Chem. Pharm. Bull.* **1990**, *38*, 285. (e) Barnard, D. L.; Hill, C. L.; Gage, T.; Matheson, J. E.; Huffman, J. H.; Sidwell, R.; Otto, M. I.; Schinazi, R. F. *Antiviral Res.* **1997**, *34*, 27. (f) Fukuda, N.; Yamase, T.; Tajima, Y. *Biol. Pharm. Bull.* **1999**, *22*, 463. (g) Rhule, J. T.; Hill, C. L.; Zheng, Z.; Schinazi, R. F. *Top. Biol. Inorg. Chem.* **1999**, *2*, 117. (h) Botto, I. M.; Barrio, D. A.; Egusquiza, M. G.; Cabello, C. I.; Cortizo, A. M.; Etcheverry, S. B. *Met. Ions Biol. Med.* **2002**, *7*, 159. (i) Wang, X.; Liu, J.; Li, J.; Yang, Y.; Liu, J.; Li, B.; Pope, M. T. *J. Inorg. Biochem.* **2003**, *94*, 279. (j) Wang, X.; Liu, J.; Pope, M. T. *Dalton Trans.* **2003**, 957.

(5) (a) Hou, Y.; Hill, C. L. *New J. Chem.* **1992**, *16*, 909. (b) Yamase, T. *Mol. Eng.* **1993**, *3*, 241. (c) Papaconstantinou, E. *Trends Photochem. Photobiol.* **1994**, *3*, 139. (d) Gómez-Romero, P.; Casañ-Pastor, N. *J. Phys. Chem.* **1996**, *100*, 12448. (e) Athanasios, M.; Hiskia, A.; Androulaki, E.; Dimitikali, D.; Papaconstantinou, E. *Phys. Chem. Chem. Phys.* **1999**, *1*, 437. (f) Yamase, T.; Prokop, P. V. *Angew. Chem., Int. Ed.* **2002**, *41*, 466. (g) Ruether, T.; Hultgren, V. M.; Timko, B. P.; Bond, A. M.; Jackson, W. R.; Wedd, A. G. *J. Am. Chem. Soc.* **2003**, *125*, 10133. (h) Hill, C. L. In *Comprehensive Coordination Chemistry II*; McCleverty, J. A., Meyer, T. J., Eds.; Elsevier Ltd.: Oxford, U.K., 2004.

(6) (a) Katsoulis, D. E. *Chem. Rev.* **1998**, *98*, 359. (b) Proust, A. *Actual. Chim.* **2000**, 55.

(7) Hu, C.; Wang, Y.; Li, Y.; Wang, E. *Chem. J. Internet* **2001**, *3*, http://web.chemistrymag.org/cji/2001/036022re.htm and references therein.

(8) For recent examples, see: (a) Han, Z.; Zhao, Y.; Peng, J.; Ma, H.; Liu, Q.; Wang, E.; Hu, N.; Jia, H. *Eur. J. Inorg. Chem.* **2005**, 264. (b) Zhen, P.-Q.; Ren, Y.-P.; Long, L.-S.; Huang, R.-B.; Zheng, L.-S. *Inorg. Chem.* **2005**, *44*, 1190. (c) Soumahoro, T.; Burkholder, E.; Ouellette, W.; Zubieta, J. *Inorg. Chim. Acta* **2005**, *358*, 606. (d) Dablemont, C.; Proust, A.; Thouvenot, R.; Afonso, C.; Fournier, F.; Tabet, J.-C. *Inorg. Chem.* **2004**, *43*, 3514. (e) Lisnard, L.; Dolbecq, A.; Mialane, P.; Marrot, J.; Sécheresse, F. *Inorg. Chim. Acta* **2004**, *357*, 845. (f) Niu, J.-Y.; Wei, M.-L.; Wang, J.-P.; Dang, D.-B. *Eur. J. Inorg. Chem.* **2004**, 160. (g) Dolbecq, A.; Mialane, P.; Lisnard, L.; Marrot, J.; Sécheresse, F. *Chem.*−*Eur. J.* **2003**, *9*, 2914. (h) Gamelas, J. A. F.; Cavaleiro, A. M. V.; Freire, C.; De Castro, B. *J. Coord. Chem.* **2001**, *54*, 35.

(9) Anderson, T. M.; Hardcastle, K. I.; Okun, N.; Hill, C. L. *Inorg. Chem.* **2001**, *40*, 6418.

(10) (a) Reinoso, S.; Vitoria, P.; Lezama, L.; Luque, A.; Gutiérrez-Zorrilla, J. M. *Inorg. Chem.* **2003**, *42*, 3709. (b) San Felices, L.; Vitoria, P.; Gutiérrez-Zorrilla, J. M.; Reinoso, S.; Etxeberria, J.; Lezama, L. *Chem.*−*Eur. J.* **2004**, *10*, 5138. (c) Reinoso, S.; Vitoria, P.; San Felices, L.; Lezama, L.; Gutiérrez-Zorrilla, J. M. *Chem.*−*Eur. J.* **2005**, *11*, 1538.

(11) (a) Kahn, O. *Molecular Magnetism*; VCH: New York, 1993. (b) Carlin, R. L. *Magnetochemistry*; Spinger-Verlag: Berlin, 1986.

(12) Tézé, A.; Hervé, G. *J. Inorg. Nucl. Chem.* **1977**, *39*, 999.

oxalic acid (25 mg, 0.2 mmol) in water (10 mL) dropwise. For **B**, to an aqueous solution (10 mL) of $CuCl_2 \cdot 2H_2O$ (34 mg, 0.2 mmol) was added 40 mL of a solution of $K_8[\alpha\text{-}SiW_{11}O_{39}]$ (644 mg, 0.2 mmol) in a sodium acetate buffer (1.0 M), and the reaction mixture was heated to 100 °C for 1 h. Solution **A** was added dropwise to solution **B**, and a blue precipitate appeared. The reaction mixture was stirred overnight, and the precipitate was then removed by filtration. Laminar blue crystals suitable for X-ray diffraction were obtained from the mother liquor by slow evaporation. Anal. Calcd for $C_{44}H_{42}Cu_5K_2N_8O_{52}SiW_{11} \cdot 14H_2O$: C, 12.54; H, 1.67; N, 2.66; Cu, 7.54; K, 1.86. Found: C, 12.45; H, 1.72; N, 2.78; Cu, 7.31; K, 1.77. IR ($cm^{-1}$): oxalate, 1649 (vs); POM, 1003 (m), 951 (m), 904 (vs), 798 (vs), 700 (s), 540 (m), 542 (m), 480 (m). TGA/DTA shows a dehydration step below 160 °C partially overlapped with the collapse of the crystal structure; it involves the loss of approximately 19 water molecules.

**Synthesis of $K_{14}[\{SiW_{11}O_{39}Cu(H_2O)\}\{Cu_2(bpy)_2(\mu\text{-}ox)\}]_2[SiW_{11}O_{39}Cu(H_2O)] \cdot 55H_2O$ (2).** The same synthetic procedure was followed using a solution of $K_8[\alpha\text{-}SiW_{11}O_{39}]$ (0.2 mmol), in a 1.0 M potassium acetate buffer. Prismatic blue crystals suitable for X-ray diffraction were obtained from the mother liquor by slow evaporation. Anal. Calcd for $C_{44}H_{38}Cu_7K_{14}N_8O_{128}Si_3W_{33} \cdot 55H_2O$: C, 4.87; H, 1.37; N, 1.03; Cu, 4.10; K, 5.04. Found: C, 4.83; H,1.36; N, 1.11; Cu, 4.03; K, 4.98. IR ($cm^{-1}$): oxalate, 1647 (s); POM, 1009 (m), 953 (s), 903 (vs), 798 (vs), 690 (s), 540 (m), 474 (m). TGA/DTA shows a dehydration step below 200 °C highly overlapped with the collapse of the crystal structure; it involves the loss of at least 52 water molecules.

**Synthesis of $(NH_4)_4[\{SiW_{11}O_{39}Cu(H_2O)\}\{Cu_2(bpy)_2(\mu\text{-}ox)\}] \cdot 10H_2O$ (3).** The same synthetic procedure was followed using a solution of $K_8[\alpha\text{-}SiW_{11}O_{39}]$ (0.2 mmol) in a 1.0 M ammonium acetate buffer. Prismatic blue crystals suitable for X-ray diffraction were obtained from the mother liquor by slow evaporation. Anal. Calcd for $C_{22}H_{34}Cu_3N_{12}O_{44}SiW_{11} \cdot 10H_2O$: C, 7.47; H, 1.54; N, 3.17; Cu, 5.39. Found: C, 7.49; H, 1.58; N, 3.05; Cu, 5.23. IR ($cm^{-1}$): oxalate, 1643 (s); POM, 1007 (m), 947 (s), 899 (vs), 795 (vs), 692 (s), 540 (m), 480 (m). TGA/DTA shows a dehydration step below 200 °C partially overlapped with the collapse of the crystal structure; it involves the loss of approximately 12 water molecules.

**Synthesis of $Rb_4[\{SiW_{11}O_{39}Cu(H_2O)\}\{Cu_2(bpy)_2(\mu\text{-}ox)\}] \cdot 10H_2O$ (4).** The same synthetic procedure was followed using a solution of $K_8[\alpha\text{-}SiW_{11}O_{39}]$ (0.2 mmol) in a 1.0 M rubidium acetate buffer. Prismatic blue crystals suitable for X-ray diffraction were obtained from the mother liquors by slow evaporation. Anal. Calcd for $C_{22}H_{18}Cu_3N_4O_{44}Rb_4SiW_{11} \cdot 10H_2O$: C, 6.94; H, 1.01; N, 1.47; Cu, 4.10; Rb, 8.98. Found: C, 6.91; H, 0.83; N, 1.49; Cu, 5.01; Rb, 8.77. IR ($cm^{-1}$): oxalate, 1643 (s); POM, 1003 (m), 947 (s), 899 (vs), 796 (vs), 690 (s), 536 (m), 478 (m). TGA/DTA shows a dehydration step below 200 °C partially overlapped with the collapse of the crystal structure; it involves the loss of approximately 13 water molecules.

**X-ray Data Collection and Structure Determination**. Room-temperature single-crystal data collection for **1** was performed on a STOE IPDS diffractometer, equipped with graphite-monochromated Mo Kα radiation ($\lambda = 0.71073$ Å) and an image-plate area detector operating in the oscillating $\varphi$-rotation mode. Unit cell refinement was based on all observed reflections from 10 frames collected with an oscillation range of 1° per frame and an exposure time of 3 min per frame. The final data collection consisted of 200 frames with an oscillation range of 1° per frame and an exposure time of 5 min per frame. Crystallographic data for compound **2** have been described previously[10a] in the *C*2/*m* space group. However, to better show the close relation between the crystal structure of **2** and that of the isostructural compounds **3** and **4**, we have exchanged the original *a* and *c* axes and inverted the *b* axis, resulting in a unit cell with the *A*2/*m* space group. Structural data for compounds **3** and **4** were collected at room temperature on an Oxford Diffraction Xcalibur diffractometer equipped with graphite-monochromated Mo Kα radiation ($\lambda = 0.71073$ Å) and a Sapphire CCD detector. A total of 1148 (920) frames of data were collected with an exposure time of 15 s per frame for compound **3**, using the $\omega$-scan technique with a frame width of $\Delta\omega = 0.40°$, and an exposure time of 10 s per frame with $\Delta\omega = 0.50°$ for compound **4**. Data frames were processed (unit cell determination, intensity data integration, correction for Lorentz and polarization effects, and analytical absorption correction) using Stoe IPDS software[13a] and X-RED[13b] for compound **1**, and the CrysAlis software package[14] for compounds **3** and **4**.

Neutral atom scattering factors and anomalous dispersion factors were taken from the literature.[15] The structures were solved using a combination of direct and Patterson methods (DIRDIF 99).[16] SHELXL97[17] was used for structure refinement of the compounds. All crystallographic calculations were performed using the WINGX software package.[18] In all compounds, copper atoms in the polyanions were delocalized over all tungsten positions except those that support a metalorganic moiety, as these must be bonded to a terminal oxo group and obviously cannot contain a copper atom bonded to a water molecule. Their population parameters were initially refined without restrictions, resulting in the expected number of one copper ion per Keggin subunit. In the last cycle of refinement, the sum of the copper population factors was restricted to one. Hydrogen atoms of the bipyridine ligands were placed in calculated positions, and were refined with a riding model.

Single crystals of all attempted syntheses of compound **1** were very thin, fragile, difficult to manipulate, and of quite low crystallinity, and started decaying immediately after being removed from solution, thus giving broad and low-intensity peaks in their X-ray diffractograms, which translated into a quite low quality of the data. After we located and refined the hybrid POM in compound **1**, the difference Fourier map showed many peaks of very low electronic density, suggesting an extensive disorder of the water solvent molecules. Thus, the solvent molecules that reside in those regions of diffuse electron density were treated by the Platon/Squeeze procedure[19] to remove the contribution of the disordered component to the structure factors; it suggested a unit cell accessible volume of about 23% containing about 275 electrons, which could accommodate the 14 water molecules per formula unit expected through the TGA measurement. This large space filled with disordered solvent is probably the main reason for the fragility of the crystals. Because of the low quality of the data, several geometric restrictions were necessary during the refinement, mostly in order to maintain planarity of the 2,2′-bipyridine and oxalate moieties, and to normalize their internal bond distances and angles

(13) (a) Stoe & Cie. *Stoe IPDS Software 2.87*; Stoe & Cie: Darmstadt, Germany, 1998. (b) Stoe & Cie. *Stoe X-RED 1.08. Data reduction for STADI4 and IPDS*; Stoe & Cie: Darmstadt, Germany, 1996.
(14) Oxford Diffraction. *CrysAlis CCD and RED*, version 1.70; Oxford Diffraction Ltd.: Oxford, U.K., 2003.
(15) *International Tables for X-ray Crystallography, Vol. IV*; Kynoch Press: Birmingham, U.K., 1974.
(16) Beurkens, P. T.; Beurkens, G.; de Gelder, R.; García-Granda, S.; Gould, R. O.; Israel, R.; Smits, J. M. M. *DIRDIF-99 Program System*; Crystallography Laboratory, University of Nijmegen: Nijmegen, The Netherlands, 1999.
(17) Sheldrick, G. M. *SHELXL97, Program for Crystal Structure Refinement*; University of Göttingen: Göttingen, Germany, 1997.
(18) Farrugia, L. J. *J. Appl. Crystallogr.* **1999**, *32*, 837.
(19) Van der Sluis, P.; Spek, A. L. *Acta Crystallogr.* **1990**, *A46*, 194.

**Table 1.** Crystallographic Data for Compounds **1**−**4**

| | **1** | **2**[a] | **3** | **4** |
|---|---|---|---|---|
| formula | $C_{44}H_{70}Cu_5K_2N_8O_{66}SiW_{11}$ | $C_{44}H_{148}Cu_7K_{14}N_8O_{183}Si_3W_{33}$ | $C_{22}H_{54}Cu_3N_8O_{54}SiW_{11}$ | $C_{22}H_{38}Cu_3N_4O_{54}Rb_4SiW_{11}$ |
| fw | 4213.4 | 10861.1 | 3535.8 | 3805.5 |
| space group | $P2_1/m$ | $A2/m$ | $P2_1/c$ | $P2_1/c$ |
| $a$ (Å) | 12.487(1) | 12.546(2) | 12.694(1) | 12.677(1) |
| $b$ (Å) | 20.582(2) | 21.303(3) | 18.935(1) | 18.933(1) |
| $c$ (Å) | 18.620(2) | 37.932(6) | 26.934(1) | 26.983(1) |
| $\beta$ (deg) | 101.78(1) | 106.16(1) | 90.194(3) | 90.138(3) |
| $V$ (Å$^3$) | 4684.6(7) | 9737(3) | 6473.7(5) | 6476.3(5) |
| $D_{cal}$ (g cm$^{-3}$) | 2.987 | 3.705 | 3.628 | 3.904 |
| $Z$ | 2 | 2 | 4 | 4 |
| $F(000)$ | 3814 | 9770 | 6356 | 6772 |
| $\mu$ (mm$^{-1}$) | 14.763 | 20.586 | 20.560 | 23.528 |
| no. of collected reflns | 30 361 | 15 207 | 40 536 | 39 843 |
| no. of unique reflns | 9265 | 14 586 | 13 886 | 12 682 |
| obsd reflns ($I > 2\sigma I$) | 2373 | 7948 | 7481 | 6474 |
| params | 307 | 618 | 697 | 692 |
| $R(F_o)$[b] (obsd reflns) | 0.0749 | 0.0705 | 0.0469 | 0.0485 |
| $wR(F_o^2)$[b] (all rflns) | 0.1982 | 0.1991 | 0.1015 | 0.1099 |
| $S$ | 0.681 | 0.945 | 0.864 | 0.854 |

[a] Previously described in space group $C2/m$. [b] $R(F_o) = \sum||F_o| - |F_c||/\sum|F_o|$; $wR(F_o^2) = \{\sum[w(F_o^2 - F_c^2)^2]/\sum[w(F_o^2)^2]\}^{1/2}$.

to the values observed in similar compounds. Besides, the central oxygens O23 and O24 were kept in fixed positions. Thermal vibrations were treated anisotropically for W and Cu atoms.

In compound **3**, W, Cu, $O_{POM}$, and ammonium N atoms were refined anisotropically. Finally, in compound **4**, two Rb cations and three water molecules were disordered over five crystallographic positions with the following population factors (%) for rubidium atoms: Rb3A, 40.8; Rb3B, 22.2; Rb3C, 52.9; Rb3D, 66.7; Rb3E, 17.4. Heavy atoms (including Rb1 and Rb2) and the O atoms belonging to the POM were refined anisotropically. Experimental details and crystal data for all four compounds are given in Table 1.

**Computational Details.** All the quantum calculations have been carried out using the Gaussian03 program[20] running on computers with a GNU/Linux operating system. Density functional theory, specifically Becke's hybrid method with three parameters[21] based on a mixture of Hartree−Fock exchange with DFT nonlocal exchange and correlation functionals, as implemented in Gaussian03 (B3LYP), has been used in all calculations.

Experimental data were used as the starting point in the global optimization of the $[\{Cu(bpy)(H_2O)_2\}(\mu\text{-ox})]^{2+}$ cationic complex ($C_{2h}$, $S = 1$). The standard 6-31G(d)[22] basis has been chosen for all atoms. This basis contains polarization functions[23] in all atoms, except hydrogen. The optimization procedure for the $[SiW_{12}O_{40}]^{4-}$ and $[SiW_{11}O_{39}\{Cu(H_2O)\}]^{6-}$ Keggin polyanions has been previously reported.[10c]

The exchange coupling constants $J_{ij}$ (defined through the phenomenological Heisenberg Hamiltonian $H_{ij} = -J_{ij}S_iS_j$) of the binuclear complexes have been calculated using the broken-symmetry computational strategy of Ruiz et al.,[24] which has been shown to provide good results as compared to experimental data. These calculations have used the experimental structure, since the calculated coupling constants are very sensitive to small deviations in the geometrical parameters. For the evaluation of the coupling constants of the copper(II) dimer complexes, two separate DFT calculations have been carried out, from which the energies of the triplet state ($E_{HS}$) and a broken-symmetry singlet configuration ($E_{BS}$) are obtained, whereupon the coupling constant is approximately

$$J_D = E_{BS} - E_{HS}$$

To calculate the coupling constants the following combination of basis sets was used: the Los Alamos effective core potential combined with a DZ basis (LANL2DZ)[25] for tungsten and silicon; Ahlrichs and co-workers'[26] valence triple-$\zeta$ basis set for copper and valence double-$\zeta$ basis set for the remaining atoms, including polarization functions for all the atoms except hydrogens.

## Results and Discussion

**Synthesis.** In contrast to most of the TM complex−POM compounds reported in the literature, which are synthesized by hydrothermal methods, compounds **1**−**4** were prepared under mild conditions by auto-assembly of the in situ generated inorganic $[SiW_{11}O_{39}\{Cu(H_2O)\}]^{6-}$ and metalorganic $[Cu_2(bpy)_2(\mu\text{-ox})]^{2+}$ building blocks, using an acetic acid/alkaline acetate buffer solution as the reaction medium.


(20) Frisch, M. J.; Trucks, G. W.; Schlegel, H. B.; Scuseria, G. E.; Robb, M. A.; Cheeseman, J. R.; Montgomery, J. A., Jr.; Vreven, T.; Kudin, K. N.; Burant, J. C.; Millam, J. M.; Iyengar, S. S.; Tomasi, J.; Barone, V.; Mennucci, B.; Cossi, M.; Scalmani, G.; Rega, N.; Petersson, G. A.; Nakatsuji, H.; Hada, M.; Ehara, M.; Toyota, K.; Fukuda, R.; Hasegawa, J.; Ishida, M.; Nakajima, T.; Honda, Y.; Kitao, O.; Nakai, H.; Klene, M.; Li, X.; Knox, J. E.; Hratchian, H. P.; Cross, J. B.; Bakken, V.; Adamo, C.; Jaramillo, J.; Gomperts, R.; Stratmann, R. E.; Yazyev, O.; Austin, A. J.; Cammi, R.; Pomelli, C.; Ochterski, J. W.; Ayala, P. Y.; Morokuma, K.; Voth, G. A.; Salvador, P.; Dannenberg, J. J.; Zakrzewski, V. G.; Dapprich, S.; Daniels, A. D.; Strain, M. C.; Farkas, O.; Malick, D. K.; Rabuck, A. D.; Raghavachari, K.; Foresman, J. B.; Ortiz, J. V.; Cui, Q.; Baboul, A. G.; Clifford, S.; Cioslowski, J.; Stefanov, B. B.; Liu, G.; Liashenko, A.; Piskorz, P.; Komaromi, I.; Martin, R. L.; Fox, D. J.; Keith, T.; Al-Laham, M. A.; Peng, C. Y.; Nanayakkara, A.; Challacombe, M.; Gill, P. M. W.; Johnson, B.; Chen, W.; Wong, M. W.; Gonzalez, C.; Pople, J. A. *Gaussian 03*, revision C.02; Gaussian, Inc.: Wallingford, CT, 2004.

(21) Becke, A. D. *J. Chem. Phys.* **1993**, *98*, 5648.

(22) (a) Hehre, W. J.; Ditchfield, R.; Pople, J. A. *J. Chem. Phys.* **1972**, *56*, 2257. (b) Francl, M. M.; Pietro, W. J.; Hehre, W. J.; Binkley, J. S.; DeFrees, D. J.; Pople, J. A.; Gordon, M. S. *J. Chem. Phys.* **1982**, *77*, 3654. (c) Rassolov, V. A.; Ratner, M. A.; Pople, J. A.; Redfern, P. C.; Curtiss, L. A. *J. Comput. Chem.* **2001**, *22*, 976.

(23) Frisch, M. J.; Pople, J. A.; Winkley, J. S. *J. Chem. Phys.* **1984**, *80*, 3265.

(24) Ruiz, E.; Alemany, P.; Álvarez, S.; Cano, J. *J. Am. Chem. Soc.* **1997**, *119*, 1297.

(25) (a) Hay, P. J.; Wadt, W. R. *J. Chem. Phys.* **1985**, *82*, 270. (b) Wadt, W. R.; Hay, P. J. *J. Chem. Phys.* **1985**, *82*, 284. (c) Hay, P. J.; Wadt, W. R. *J. Chem. Phys.* **1985**, *82*, 299.

(26) (a) Schaefer, A.; Horn, H.; Ahlrichs, R. *J. Chem. Phys.* **1992**, *97*, 2571. (b) Schaefer, A.; Huber, C.; Ahlrichs, R. *J. Chem. Phys.* **1994**, *100*, 5829.

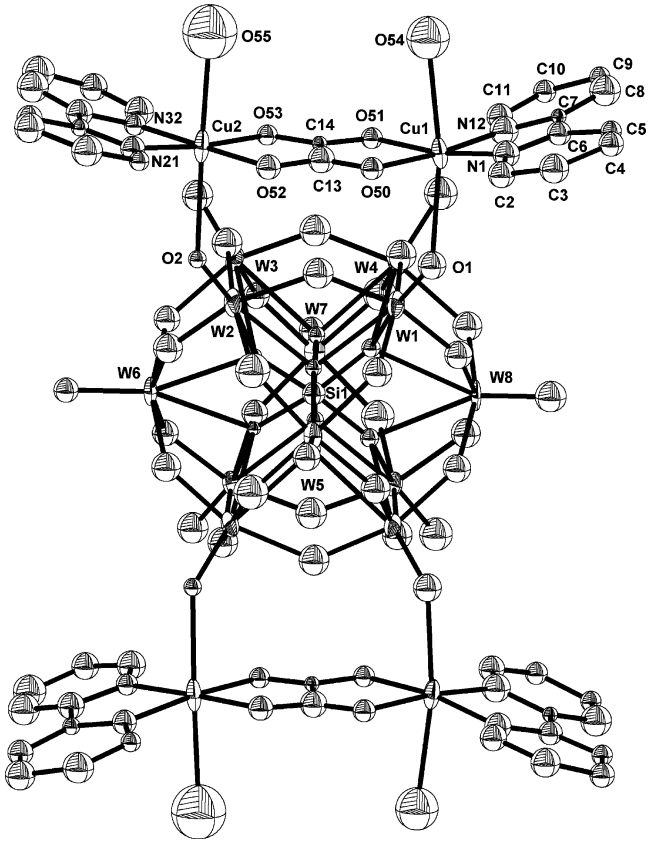


**Figure 1.** ORTEP view of the $[\{SiW_{11}O_{39}Cu(H_2O)\}\{Cu_2(bpy)_2(H_2O)_2(\mu\text{-ox})\}_2]^{2-}$ anion (**1**) with atom labeling. The copper atom is delocalized over the W3−W8 sites. This molecule has a crystallographic $C_s$ symmetry.

The syntheses of the four compounds were carried out under the same reaction conditions with the exception of the alkaline cation employed in the buffered acetate medium. This variable has a decisive influence in both the composition (alkaline countercation and POM:dimer ratio) and the dimensionality of the final compound.

The $\mu$-oxalatodicopper complex shows a strong tendency to coordinate to the Keggin polyanion because its anchorage to the inorganic building block takes place regardless of the reaction medium. Moreover, it tends to act as a bridge between Keggin subunits to give monodimensional $[\{SiW_{11}O_{39}Cu(H_2O)\}\{Cu_2(bpy)_2(\mu\text{-ox})\}]_n^{4n-}$ hybrid polyanions. Thus, when ammonium or rubidium buffers are employed, these cations replace the potassium of the $K_8[SiW_{11}O_{39}]$ POM precursor to give two isostructural salts of this polymeric POM (**3** and **4**, respectively), whereas the final compound obtained from the potassium buffer (**2**) contains noncoordinated $[SiW_{11}O_{39}\{Cu(H_2O)\}]^{6-}$ anions besides the polymeric POM. [10a] In contrast, neither the bridging behavior of the metalorganic block nor the cation metathesis is observed when the sodium buffer is used, and therefore a potassium salt of the discrete $[\{SiW_{11}O_{39}Cu(H_2O)\}\{Cu_2(bpy)_2(H_2O)_2(\mu\text{-ox})\}_2]^{2-}$ hybrid polyanion (**1**) is obtained.

**Description of the Structures.** Compound **1** contains the discrete hybrid polyanion $[\{SiW_{11}O_{39}Cu(H_2O)\}\{Cu_2(bpy)_2(H_2O)_2(\mu\text{-ox})\}_2]^{2-}$ (Figure 1), whereas the polymeric hybrid polyanion $[\{SiW_{11}O_{39}Cu(H_2O)\}\{Cu_2(bpy)_2(\mu\text{-ox})\}]_n^{4n-}$ gives a monodimensional character to compounds **2**−**4**. The main

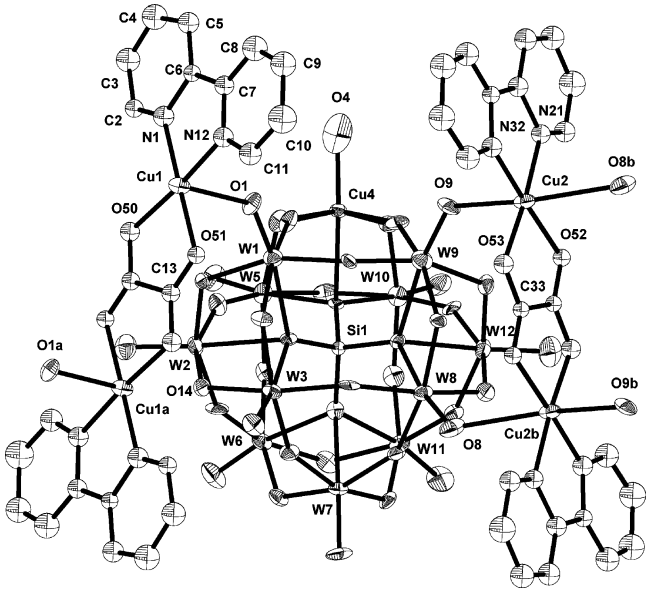


**Figure 2.** ORTEP view of the $[\{SiW_{11}O_{39}Cu(H_2O)\}\{Cu_2(bpy)_2(\mu\text{-ox})\}_2]^{4-}$ fragment present in compounds **3** and **4** with atom labeling and showing the different attachment of the two $\mu$-oxalatodicopper complexes to the POM.

structural feature of these compounds is the presence of copper(II)-monosubstituted α-Keggin polyoxoanions as inorganic building blocks, on which the $\mu$-oxalatodicopper metalorganic blocks are supported. Figure 2 shows the ORTEP views of the hybrid polyanions of compounds **3** and **4**. On the other hand, compound **2** contains both polymeric hybrid polyanions and free $[SiW_{11}O_{39}Cu(H_2O)]^{6-}$ POMs. Although its crystal structure was previously solved in the *C*2/*m* space group,[10a] here we report its solution in the *A*2/*m* space group, which allows for a better comparison with the crystal structures of compounds **3** and **4**.

The inorganic building block $[\alpha\text{-}SiW_{11}O_{39}Cu(H_2O)]^{6-}$ consists of a central $SiO_4$ tetrahedron surrounded by four vertex-sharing $M_3O_{13}$ trimers, which result from the association of three edge-sharing $MO_6$ octahedra in such a way that the ideal polyanion has $C_s$ symmetry. The copper atom is disordered over the whole polyanion, except for the octahedra on which the metalorganic blocks are supported. A preferential position is observed on the Cu4 site for compounds **2**−**4** (56% for **2**, 44% for **3**, and 52% for **4**), whereas in compound **1** all population factors are less than 20%. The M−O bond lengths in all compounds are not unusual, but it is worth mentioning that the Jahn−Teller effect associated with the octahedral copper(II) ions induces an elongation of the monosubstituted Keggin anions along the $Cu-W_{trans}$ direction. Moreover, the different coordination spheres for copper(II) and tungsten(VI) centers produce a distortion in the whole skeleton of the Keggin anion consisting of a sequence of alternating long and short equatorial M−O bonds whose propagation starts at the Cu center and attenuates toward the $W_{trans}$ atom[10c] (Table 2).

The metalorganic building blocks are made of two copper atoms bridged by an oxalate anion in the usual bis(bidentate) fashion. These $\mu$-oxalatodicopper complexes are centrosymmetric in compounds **2**, **3**, and **4**. The copper atoms are

**Table 2.** Ranges of M−O[a] Bond Distances in Compounds **1**−**4** Compared with Those of $[SiW_{11}O_{39}Cu(H_2O)]^{6-}$ (**$SiW_{11}Cu$**) and $[SiW_{12}O_{40}]^{4-}$ (**$SiW_{12}$**) Optimized Polyanions

| | **1** | **2** | **3** | **4** | **$SiW_{11}Cu$** | **$SiW_{12}$** |
|---|---|---|---|---|---|---|
| W−$O_c$ | 2.27−2.51 | 2.29−2.38 | 2.29−2.35 | 2.28−2.37 | 2.32−2.44 | 2.325 |
| W−$O_b$ | 1.78−2.06 | 1.85−2.01 | 1.85−2.00 | 1.84−2.00 | 1.81−2.03 | 1.916, 1.937 |
| W−$O_t$ | 1.61−1.86 | 1.70−1.79 | 1.70−1.80 | 1.70−1.78 | 1.76−1.77 | 1.743 |
| Si−$O_c$ | 1.53−1.63 | 1.62−1.64 | 1.63−1.65 | 1.63−1.66 | 1.63−1.66 | 1.667 |
| Cu−$O_c$ | | 2.35 | 2.34 | 2.31 | 2.319 | |
| Cu−$O_b$ | | 1.91, 198 | 1.92−1.97 | 1.92−1.96 | 2.011, 2018 | |
| Cu−$O_t$ | | 2.01 | 1.88 | 1.89 | 2.286 | |
| Cu···Si | | 3.49 | 3.50 | 3.48 | 3.377 | |
| Si···$W_{trans-Cu}$ | | 3.49 | 3.49 | 3.50 | 3.589 | |
| W···Si | 3.49−3.54 | 3.50−3.53 | 3.50−3.54 | 3.49−3.54 | 3.56−3.64 | 3.588 |
| Cu···$W_{trans}$ | | 6.98 | 6.99 | 6.97 | 6.964 | |
| W···$W_{trans}$ | 7.03−7.05 | 7.02−7.03 | 7.00−7.07 | 6.99−7.06 | 7.15−7.21 | 7.172 |
| $O_{Cu}$···$O_{W-trans}$ | | 10.62 | 10.54 | 10.51 | 10.709 | |
| O···$O_{trans}$ | 10.30−10.62 | 10.30−10.47 | 10.38−10.49 | 10.38−10.48 | 10.61−10.69 | 10.619 |

[a] $O_c$, oxygen atoms belonging to the central $SiO_4$ tetrahedron; $O_b$, bridging oxygen atoms between $MO_6$ octahedra; $O_t$, terminal oxygen atoms.

involved in $CuN_2O_2O'O''$ chromophores in elongated octahedral environments, in which two oxalate oxygen atoms and two bipyridine nitrogen atoms occupy the equatorial positions. In compound **1**, two dicopper complexes are supported over mirror-plane-related $W_2O_{10}$ dimers belonging to a Keggin anion, in such a way that the apical positions of each copper atom are occupied by a terminal oxygen atom and a water molecule, giving rise to the discrete hybrid polyanion $[\{SiW_{11}O_{39}Cu(H_2O)\}\{Cu_2(bpy)_2(H_2O)_2(\mu\text{-ox})\}_2]^{2-}$. On the other hand, in the rest of the compounds, they are lying over $W_3O_{13}$ trimers through axial coordination to terminal or bridging oxygen atoms. The shorter $Cu-O_{apical}$ distance is always of type $Cu-O_t$, so the dicopper complex may be considered as coordinated to terminal oxygen atoms and semicoordinated, or even noncoordinated, to bridging ones. This type of linking between building blocks produces zigzagging chains built of alternating POMs and $\mu$-oxalatodicopper complexes. It is worth mentioning that the interactions between these building blocks through bridging oxygen atoms are very labile. This makes the hybrid chains flexible enough to adopt the different conformations imposed by the crystal packing. Thus, some differences can be appreciated between the hybrid chains of compound **2** and those present in compounds **3** and **4**. In compound **2**, the entire metalorganic blocks are supported over the center of a trimer, and are linked by both terminal and bridging oxygens, whereas alternating metalorganic moieties in compounds **3** and **4** are shifted toward the edge of the corresponding trimer, resulting in a replacement of the bridging oxygen by a terminal one, and consequently in a stronger link to the POM. The rest of the dicopper complexes remain in the same relative positions with a slight shortening of the $Cu-O_t$ bond and a significant lengthening of the $Cu-O_b$ distance, so the coordination sphere of the copper atom can be best described as a square pyramid. These different types of connectivity between building blocks produce a pronounced decrease in the hybrid chain zigzagging angle when going from compound **2** to **3** or **4** (Figure 3).

The Cu−oxalato−Cu framework in compound **1** adopts a boat conformation, similar to that observed in the chloro-complex $[\{CuCl(bpy)\}_2(ox)]$.[27] This is probably due to the linkage of the dicopper complex to the Keggin subunit by

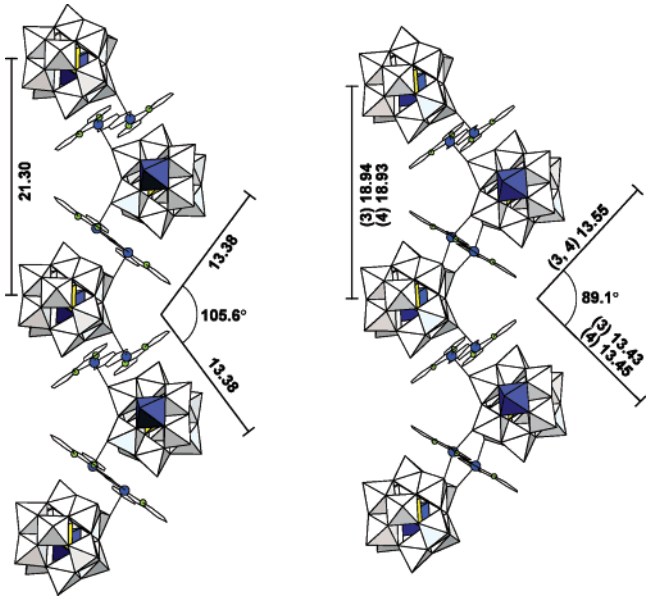


**Figure 3.** Selected Si···Si distances (Å) and zigzagging angle in the chains of polymeric compounds **2** (left) and **3** and **4** (right).

one of its faces, and it favors both $\pi$-stacking interactions between the bipyridine ligands and a more-compact packing of the POMs. On the other hand, the bridging function of the dicopper complexes in compounds **2**, **3**, and **4** seems to be the reason for their quasi-planarity. Both boat and planar conformations are not usual for $\mu$-oxalatodicopper complexes, and they contrast with the chair conformation the Cu−oxalato−Cu framework adopts for the DFT-optimized $[\{Cu(bpy)(H_2O)_2\}_2(ox)]^{2+}$ cationic complex. Table 3 displays selected bond distances and angles of the metalorganic blocks together with the optimized values.

**Packing of Compound 1.** The crystal structure of compound **1** is composed of hybrid $[\{SiW_{11}O_{39}Cu(H_2O)\}\{Cu_2(bpy)_2(H_2O)_2(\mu\text{-ox})\}_2]^{2-}$ polyanions bridged by K1 and presumably K2 cations and water molecules, forming chains parallel to the [100] direction (Figure 4). Each chain is connected to its four nearest neighbors through $\pi$-stacking interactions between bipyridine aromatic rings, and to two

(27) Chattopadhyay, S. K.; Seth, S.; Mak, T. C. W. *J. Coord. Chem.* **2002**, *55*, 259.

**Table 3.** Selected Bond Distances (Å) and Angles (deg) for the Metalorganic Building Blocks of Compounds **1**−**4**, Together with the Optimized Values for $[\{Cu(bpy)(H_2O)_2\}_2(ox)]^{2+}$ [a]

| | Cu1 coordination sphere[b] | | | | | Cu2 coordination sphere | | | |
|---|---|---|---|---|---|---|---|---|---|
| | **1** | **2** | **3** | **4** | | **1** | **3** | **4** | optimized |
| Cu1−O50 | 2.03(2) | 1.96(1) | 1.98(1) | 1.98(1) | Cu2−O52 | 1.97(3) | 1.99(1) | 1.99(1) | 1.966 |
| Cu1−O51 | 1.95(2) | 1.98(1) | 1.98(1) | 2.00(1) | Cu2−O53 | 1.90(2) | 1.96(1) | 1.95(1) | 1.966 |
| Cu1−N1 | 1.96(3) | 1.97(2) | 1.99(1) | 1.98(2) | Cu2−N21 | 2.00(2) | 1.96(1) | 2.00(2) | 1.980 |
| Cu1−N12 | 1.90(2) | 1.96(2) | 2.01(1) | 2.02(2) | Cu2−N32 | 1.93(2) | 1.98(1) | 1.98(2) | 1.980 |
| Cu1−O1 | 2.47(3) | 2.54(2) | 2.42(1) | 2.38(1) | Cu2−O9 | | 2.50(1) | 2.53(1) | 2.315 |
| Cu1−O54 | 2.59(4) | | | | Cu2−O2 | 2.49(2) | | | |
| Cu1···O14[(i)] | | 2.94(1) | 3.20(1) | 3.16(1) | Cu2−O55 | 2.60(6) | | | |
| Cu1···Cu1[(i)] | | 5.147(4) | 5.167(3) | 5.158(3) | Cu2−O8[(ii)] | | 2.60(1) | 2.52(1) | 2.997 |
| Cu1···Cu2 | 5.16(2) | | | | Cu2···Cu2[(i)] | | 5.196(3) | 5.189(3) | 5.120 |
| O50−Cu1−O51 | 85.2(9) | 85.1(5) | 84.7(4) | 84.8(5) | O52−Cu2−O53 | 84.1(9) | 84.1(4) | 83.5(5) | 85.5 |
| N1−Cu1−N12 | 83.6(10) | 83.6(6) | 82.8(5) | 83.2(6) | N21−Cu2−N32 | 81.8(10) | 82.5(5) | 81.7(6) | 82.6 |
| O50−Cu1−N12 | 173.9(12) | 177.3(6) | 173.4(5) | 174.0(5) | O52−Cu2−N32 | 178.3(9) | 175.4(5) | 174.9(5) | 164.0 |
| O51−Cu1−N1 | 170.7(12) | 178.5(6) | 177.5(5) | 178.6(6) | O53−Cu2−N21 | 173.9(10) | 174.7(5) | 175.3(5) | 164.0 |
| O1−Cu1−O14[(i)] | | 173.2(4) | 164.0(3) | 164.2(4) | O9−Cu2−O8[(ii)] | | 150.3(3) | 151.9(4) | 162.2 |
| O1−Cu1−O54 | 169.4(10) | | | | O2−Cu2−O55 | 173.1(15) | | | |
| Cu1−bpy1[c] | 13.0(9) | 5.6(5) | 3.1(4) | 3.4(5) | Cu2−bpy2 | 12.1(9) | 4.6(4) | 4.4(5) | 7.2 |
| Cu1−ox1 | 6.2(9) | 1.3(5) | 2.0(4) | 2.6(5) | Cu2−ox2 | 5.2(9) | 3.3(4) | 2.4(5) | 18.2 |
| bpy1−ox1 | 18.9(9) | 5.3(5) | 4.5(4) | 4.6(5) | bpy2−ox2 | 17.3(9) | 5.3(4) | 6.3(5) | 25.4 |
| $T_d$ distortion[d] | 4.6(9) | 3.0(5) | 7.1(4) | 5.8(5) | $T_d$ distortion | 5.0(9) | 7.0(4) | 6.4(5) | |

[a] Symmetry codes: (i) **2**: $2-x, {}^1/_2-y, {}^1/_2-z$; **3**, **4**: $2-x, -y, -z$; (ii) $2-x, 1-y, -z$. [b] In compound **1**, Cu1 and Cu2 are located in the same dinuclear copper complex, whereas in compounds **3** and **4**, Cu1 and Cu2 belong to two different centrosymmetric complexes. [c] Dihedral angles between planes are defined by those atoms listed below. Cu1: O50, O51, N1, N12; ox1: O50, O51, C13, O50[(i)], O51[(i)], C13[(i)]; bpy1: N1, N12, C2−C11; Cu2: O52, O53, N21, N32; ox2: O52, O53, C33, O52[(ii)], O53[(ii)], C33[(ii)]; bpy2: N21, N32, C22−C31. In compound **1**, ox1 = ox2: O50, O51, O52, O53, C13, C14. [d] Defined by the torsion angles: N1, N12, O50, O51 (Cu1) and N21, N32, O52, O53 (Cu2).

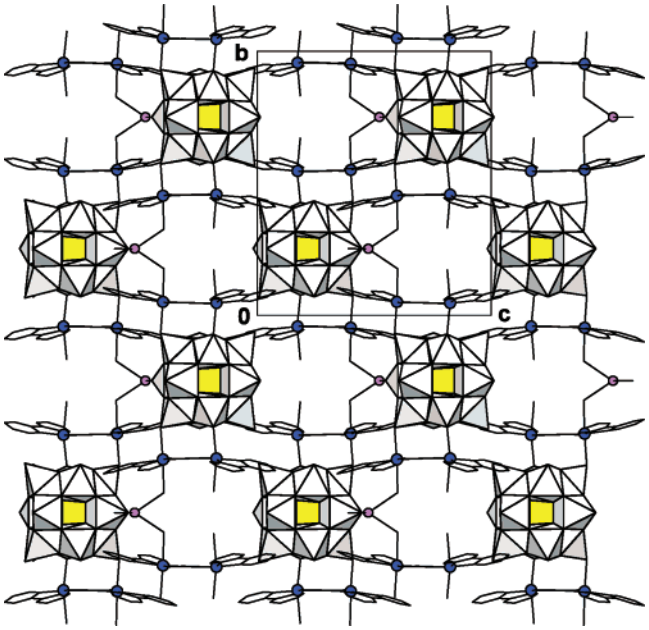


**Figure 4.** View of the chessboardlike arrangement in compound **1** showing the channels along the [100] direction.

of them also by means of the K1 coordination sphere. This chessboardlike arrangement generates quasi-rectangular channels of 10 × 8 Å$^2$ along the [100] direction. These channels are defined by two POM tetramers and two concave dicopper complexes, and they host highly disordered hydration water molecules.

**Packing of Compounds 2−4**. As can be seen in Figure 5, the packing of compound **2** is closely related to that of compounds **3** and **4**. All three compounds are formed by layers of zigzagging $[\{SiW_{11}O_{39}Cu(H_2O)\}\{Cu_2(bpy)_2(\mu\text{-}ox)\}_2]_n^{4n-}$ hybrid chains, which are arranged along the *b* axis and connected by means of the corresponding alkaline

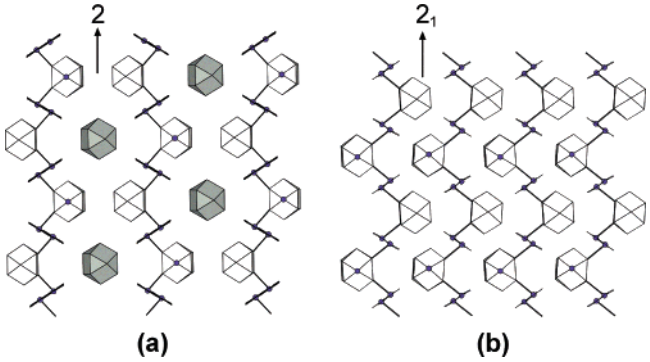


**Figure 5.** Schematic view of (a) the arrangement of the hybrid chains and free POMs in compound **2**; (b) the hybrid chain arrangement in compound **3** (or **4**).

cations. However, some differences in the relative arrangement of the hybrid chains can be appreciated: in compound **2**, the chains are related by a 2-fold axis forming elliptical spaces in the same plane, big enough to accommodate discrete $[SiW_{11}O_{39}Cu(H_2O)]^{6-}$ Keggin POMs; in compounds **3** and **4**, the chains are related by a $2_1$ axis, and there is not any free room in the layer.

In the three compounds, the hybrid layers are placed parallel to the *yz* plane with the bipyridine ligands pointing to the interlamellar space, in such a way that the layers are linked by means of $\pi$-stacking interactions through the bipyridine aromatic rings. However, some variations in the crystal packing type can be observed. Thus, while the arrangement of the chains in compounds **3** and **4** leads to a quite compact material, compound **2** shows an open structure because only with its arrangement is the formation of interlamellar cavities possible, as the bypiridine rings are located sufficiently far away (Figure 6). Moreover, the different leaning angle of the chains with regard to the *yz* plane (12° for **2** and 20° for **3** and **4**) contributes to the

**Table 4.** Spin Hamiltonian Parameters for Isolated $Cu^{II}$ Ions in the Keggin Subunits of Compounds **1**−**4**

| | **1** | | **2** | | **3** | | **4** | |
|---|---|---|---|---|---|---|---|---|
| | Q (120 K) | X (4.2 K) | Q (120 K) | X (4.2 K) | Q (120 K) | X (4.2 K) | Q (120 K) | X (4.2 K) |
| $g_{\|\|}$ | 2.425 | 2.423 | 2.430 | 2.425 | 2.423 | 2.422 | 2.423 | 2.421 |
| $g_{\perp}$ | 2.092 | 2.088 | 2.093 | 2.090 | 2.095 | 2.096 | 2.097 | 2.096 |
| $\langle g \rangle$ | 2.203 | 2.200 | 2.205 | 2.202 | 2.204 | 2.205 | 2.206 | 2.205 |
| $A_{\|\|}$ ($\times 10^{-4}$ cm$^{-1}$) | 95 | 100 | 95 | 100 | 95 | 100 | 95 | 100 |
| $A_{\perp}$ ($\times 10^{-4}$ cm$^{-1}$) | 28 | 25 | 28 | 28 | 28 | 28 | 28 | 28 |

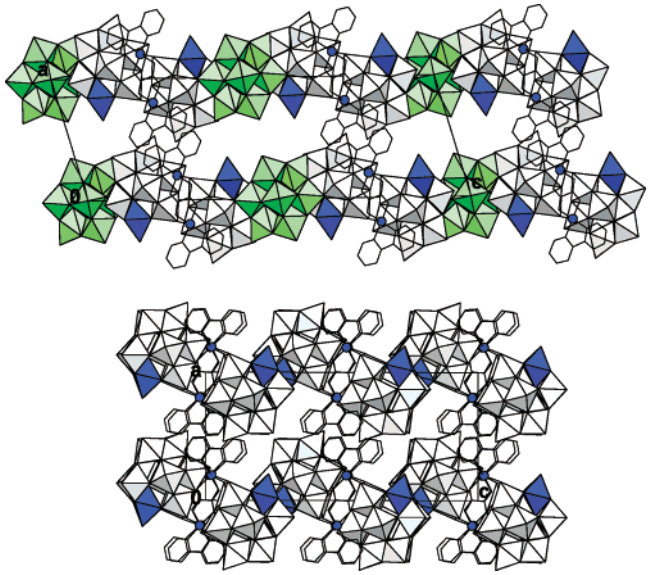

**Figure 6.** Packing of hybrid layers along the *a* axis in compound **2** (top) and **3** and **4** (bottom).

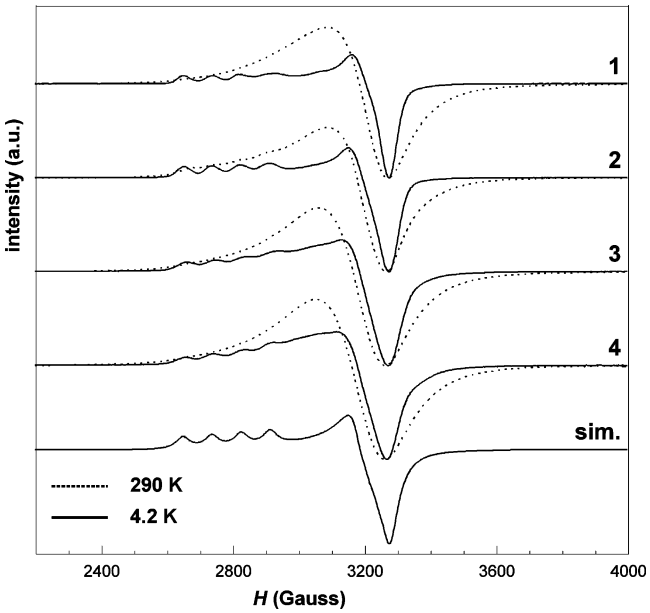


**Figure 7.** X-Band EPR powder spectra for compounds **1**−**4** registered at 290 K (dashed line) and 4.2 K (continuous line), together with the simulated spectrum for an isolated $Cu^{II}$ ion.

formation of these quasi-trapezoidal interlamellar cavities only in compound **2**.

**EPR Spectroscopy.** The thermal evolution from 290 to 4.2 K of the X-band powder spectra is similar for compounds **1**−**4** (Figure 7). The room-temperature spectra display an anisotropic broad resonance centered at ca. 3200 G. When the systems are cooled, the resolution improves considerably, as a result of the signal narrowing induced apparently by the increasing spin−lattice relaxation time. Below 100 K, the central line gives rise to an axial signal that clearly shows, in the low-field region, the hyperfine splitting originated by a spin doublet $S = 1/2$ interacting with a single $I = 3/2$ nucleus. This type of signal is characteristic of an isolated $Cu^{II}$ chromophore with an axial **g** tensor, and therefore it must originate in the $Cu^{II}$-monosubstituted Keggin POMs.

The spin Hamiltonian parameters of this monomeric contribution were estimated by comparison of the low-temperature X-band spectra with those generated by a computer simulation program working at the second order of perturbation theory. The simulation of all the spectra was satisfactory, and the best-fit results correspond to compound **2** because of the presence of noncoordinated $[SiW_{11}O_{39}Cu(H_2O)]^{6-}$ anions. The values obtained for the principal components of the **g** and **A** tensors (Table 4) are in good agreement with those observed in the potassium salts of the $Cu^{II}$-monosubstituted Keggin tungstophosphate and -silicate.[28] They are typical of octahedrally coordinated $Cu^{II}$ ions with the unpaired electron on the $d_{x^2-y^2}$ orbital. Moreover, the high $g_{||}$ value indicates a low Jahn−Teller distortion associated with the $Cu^{II}$ ion because of the rigidity imposed on its coordination sphere by the pentadentate monolacunary Keggin ligand.

The X-band powder spectra do not provide any clear information about the contribution of the copper−oxalate dimers, and therefore Q-band powder spectra were registered between 290 and 120 K (Figure 8). At room temperature, two different signals are clearly detected. One of them, with axial resolution and hyperfine splitting, is the same as that identified on the low-temperature X-band spectra, and it was simulated using the spin Hamiltonian parameters given in Table 4. The other is a broad signal, centered at ca. 11 500 G, that rapidly disappears as the temperature is lowered; it can be attributed to the copper−oxalate dimers, with the strong antiferromagnetic interaction being responsible for the decreasing intensity with decreasing temperature. In addition, the spectra of compound **1** show extra shoulders at ca. 10 800 and 11 800 G, indicating the presence of paramagnetic impurities.

The signal originating from the copper−oxalate dimers does not correspond to an isolated triplet $S = 1$ state, and therefore a nonnegligible magnetic interaction must take place between them. Considering that the $\pi$-stacking between the aromatic ligands seems to be ineffective in transmitting

(28) (a) Scholz, G.; Lück, R.; Stösser, R.; Lunk, H.-J.; Ritschl, F. *J. Chem. Soc., Faraday Trans.* **1991**, *87*, 717. (b) Gamelas, J. A.; Santos, I. C. M. S.; Freire, C.; de Castro, B.; Cavaleiro, A. M. V. *Polyhedron* **1999**, *18*, 1163.

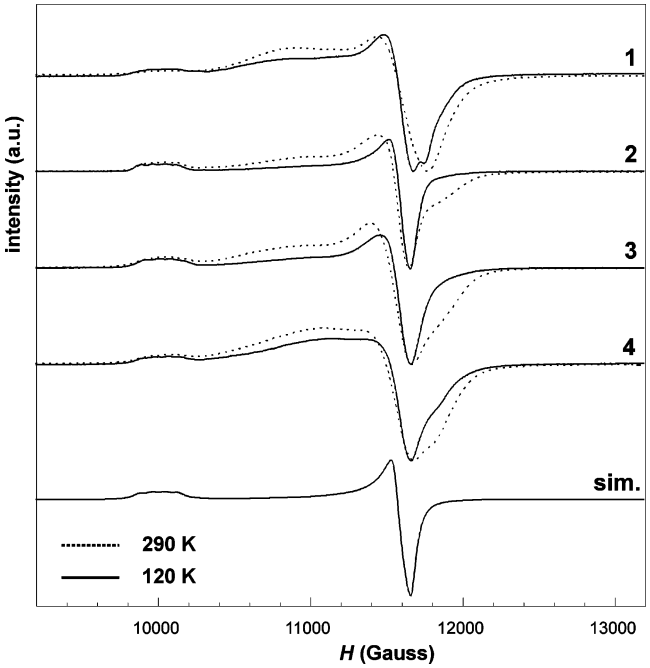


**Figure 8.** Q-Band EPR powder spectra for compounds **1**−**4** registered at 290 K (dashed line) and 120 K (continuous line), together with the expected contribution of the $Cu^{II}$-monosubstituted Keggin POMs.

magnetic interactions, the exchange pathway must involve the $[SiW_{11}O_{39}Cu(H_2O)]^{6-}$ subunits that bridge the $[Cu_2(bpy)_2(\mu\text{-ox})]^{2+}$ entities. To clarify this hypothesis, we performed Q-band single-crystal experiments on compound **4**. Figure 9 displays the angular dependence and the thermal variation of the normalized spectra corresponding to a single crystal disposed over the (001) face. At room temperature, the spectra show two types of resonances: an intense broad signal with a weak angular dependence, and a set of at least four narrower and less-intense signals whose positions undergo pronounced displacements as the angle is varied. When the system is cooled, the intensity of the broad signal rapidly diminishes, and it almost vanishes at 120 K. In contrast, the resolution of the set of signals significantly improves, and the hyperfine structure becomes resolved for some of them.

The thermal variation of the broad signal allows for its assignment to the copper−oxalate dimers, and its being a single resonance confirms the existence of interdimeric magnetic interactions. On the other hand, each of the remaining signals has its origin in the $Cu^{II}$ ion of the Keggin POM when it occupies octahedra with different orientations relative to the applied field. Their pronounced angular dependence and the observation of hyperfine structures at low temperature indicate that the $Cu^{II}$ ion is magnetically isolated in these positions. The relative intensity of the signals should be proportional to the copper population of the octahedra. The $Cu^{II}$ ion of Keggin POM in compound **4** shows a preferential position for the Cu4 octahedron (52%), the second most-populated position being the W12 octahedron (9%). Thus, a signal five times more intense than the others should be a priori expected. However, the Q-band single-crystal spectra do not show such a considerable difference in the relative intensities of the signals attributed

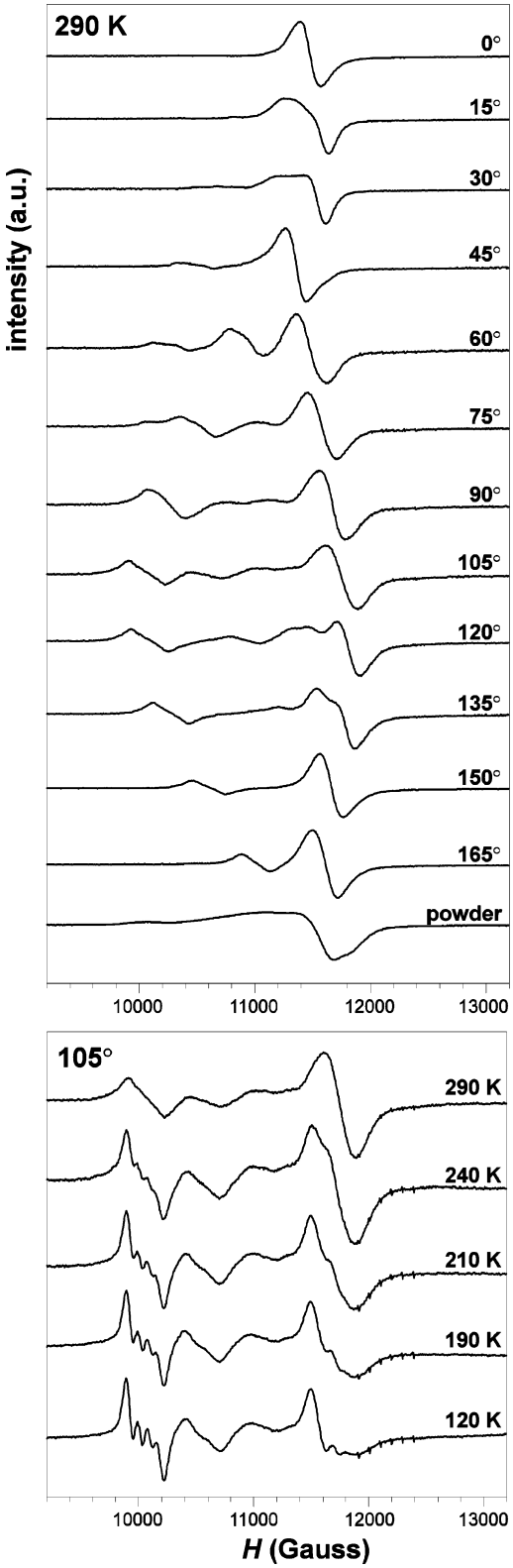


**Figure 9.** Angular dependence (top) and thermal variation (bottom) of the Q-band EPR single-crystal spectra for compound **4**.

to the monomeric contribution, and therefore none of them can originate from the $Cu^{II}$ ion when it occupies the Cu4 octahedron. This would indicate that the interdimeric interactions take place through the triad that supports the copper−oxalate dimers, in such a way that the $Cu^{II}$ POM ion in the Cu4 position is involved in the exchange pathway, whereas

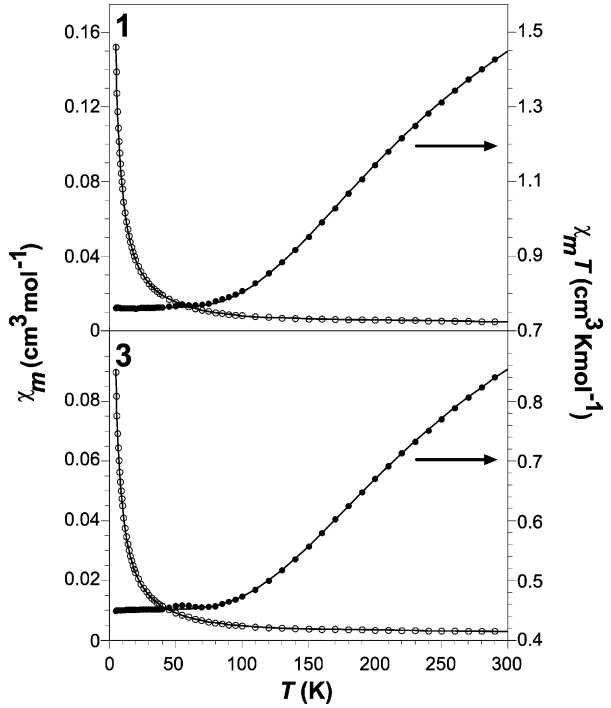


**Figure 10.** Thermal evolution of the magnetic susceptibility and $\chi_m T$ product for compounds **1** and **3**. Continuous lines represent the least-squares fit to eq 1.

it remains magnetically isolated when it occupies any other octahedra. This observation is supported by the comparison of the relative intensities of the monomeric and dimeric contributions in the Q-band powder spectra of compounds **3** and **4** (Figure 8). These compounds are isostructural, and therefore identical spectra should be a priori expected; however, the monomeric contribution in compound **4** is less intense than that in compound **3**, in line with the fact that in the former, the population of $Cu^{II}$ on the Cu4 octahedron is larger than in the latter.

**Magnetic Properties.** The thermal evolution of the magnetic molar susceptibility and the $\chi_m T$ product ($\chi_m T = \mu_{eff}^2/8$) show similar trends for compounds **1**−**4** (Figure 10). The $\chi_m$ curve increases continuously with decreasing temperature, and neither a maximum nor a Curie−Weiss behavior is observed, even at high temperatures. The room temperature $\chi_m T$ values (**1**, 1.454; **2**, 2.214; **3**, 0.856; **4**, 0.853 cm$^3$ K mol$^{-1}$) are substantially lower than those expected for as many $Cu^{II}$ ions as the molecular formulas contain, considering them to be uncoupled ions with $g = 2$ (**1**, 1.875; **2**, 2.625; **3** and **4**, 1.125 cm$^3$ K mol$^{-1}$). When the systems are cooled, the $\chi_m T$ product rapidly decreases from 300 to ca. 80 K, and remains approximately constant below 80 K. The values of the $\chi_m T$ product at 5 K (**2**, 1.361; **3**, 0.448; **4**, 0.444 cm$^3$ K mol$^{-1}$) agree with the presence of three (**2**) and one (**3** and **4**) noncoupled $Cu^{II}$ ions. In the case of compound **1**, the low-temperature $\chi_m T$ value (0.760 cm$^3$ K mol$^{-1}$) is much higher than that expected for one $Cu^{II}$ ion belonging to the Keggin POM, probably due to the contribution of the paramagnetic impurities detected by EPR spectroscopy.

This behavior indicates the presence of very strong antiferromagnetic interactions between the $Cu^{II}$ ions that form part of the $Cu^{II}$−oxalate dimers, whereas the $Cu^{II}$-monosubstituted Keggin subunits show a paramagnetic behavior, which dominates below 80 K. In this situation, the expected local maximum in the $\chi_m$ curve could either be reached out of the measured temperature range or be masked by the POM paramagnetism.

The experimental curves have been compared with those calculated with the following general expression

$$\chi_m = A\left[\frac{(1-\rho)Ng^2\beta^2}{kT[3+\exp(-J/kT)]} + \frac{\rho Ng'^2\beta^2}{4kT}\right] + B\frac{Ng'^2\beta^2}{4kT} \quad (1)$$

where $N$, $\beta$, and $k$ have their usual meanings, $g$ is the average $g$-factor of the copper−oxalate dimers, and $g'$ is the local $g$-factor of the $Cu^{II}$-monosubstituted Keggin POMs. The first term in the above expression is the classical Bleaney−Bowers equation for a dinuclear $Cu^{II}$ complex,[29] expressed per copper atom and modified to take into account the presence of noncoupled impurities. The singlet−triplet energy gap ($J$) is defined by the Hamiltonian $H = -JS_AS_B$ ($S_A = S_B = 1/2$), whereas $\rho$ is the fraction of noncoupled impurity. As shown by EPR spectroscopy, compounds **2**−**4** are almost free of noncoupled impurities, and therefore $\rho$ was fixed to zero during the fitting process. The last term corresponds to the paramagnetic contribution of the $Cu^{II}$-monosubstituted POMs. To reduce the high number of magnetic variables for compound **1**, we fixed the $g'$ value to 2.20, as deduced from the EPR powder spectra. The $A$ and $B$ factors represent the number of $Cu^{II}$ ions belonging to dimeric and monomeric species, respectively (**1**, $A = 4$ and $B = 1$; **2**, $A = 4$ and $B = 3$; **3** and **4**, $A = 2$ and $B = 1$).

It is well-known that the $\mu$-oxalatodicopper(II) complexes in which the equatorial planes are almost coplanar with the oxalate ligand exhibit strong antiferromagnetic interactions.[11,30] The Cu-equatorial $d_{x^2-y^2}$ magnetic orbital is directed toward the oxalate frontier orbitals; the antiferromagnetic contribution is therefore maximized, and $J$ values ranging from −300 to −400 cm$^{-1}$ are usually observed. Compounds **1**−**4** contain dimers with this type of topology that are magnetically coupled, as shown by the powder and single-crystal EPR spectra. The magnitude of the interdimeric coupling through the Keggin POMs is expected to be negligible in comparison with the intradimeric one, and therefore interdimeric interactions have been intentionally suppressed from eq 1 in order to avoid an excessive number of variables.

Least-squares fits of eq 1 to the experimental data were performed by minimizing the following function

$$R = \{\sum_{i=1}^{NP}[\chi_m(\exp)_i - \chi_m(\mathrm{cal})_i]^2/(NP - NV)\}^{1/2} \quad (2)$$

(29) Bleaney, B.; Bowers, K. D. *Proc. R. Soc. London, Ser. A* **1952**, *214*, 451.

(30) (a) Cano, J.; Alemany, P.; Álvarez, S.; Verdaguer, M.; Ruiz, E. *Chem.—Eur. J.* **1998**, *4*, 476. (b) Álvarez, S.; Julve, M.; Verdaguer, M. *Inorg. Chem.* **1990**, *29*, 4500.

**Table 5.** Least-Squares-Fitted Experimental and DFT-Calculated Coupling Constants ($cm^{-1}$) for the $\mu$-Oxalatodicopper Complexes in Compounds **1**−**4**

| | $g$ | $J_{exp}$ | $J_{DFT1}$[a] | $J_{DFT2}$[a] | $g'$ | $\rho$ | $R$ ($\times 10^4$) |
|---|---|---|---|---|---|---|---|
| **1** | 2.13 | −340.8 | −375.0 | −298.4 | 2.20 | 0.180 | 4.03 |
| **2** | 2.13 | −350.0 | −422.3 | | 2.21 | | 4.22 |
| **3** | 2.12 | −351.0 | −419.6 (Cu1) | −309.2 (Cu1) | 2.19 | | 4.15 |
| | | | −419.7 (Cu2) | −314.0 (Cu2) | | | |
| **4** | 2.11 | −352.9 | | | 2.18 | | 4.17 |

[a] Model DFT1 corresponds to a fragment containing two $[SiW_{12}O_{40}]^{4-}$ Keggin subunits bridged by a $[\{Cu(bpy)\}_2(\mu\text{-ox})]^{2+}$ dimer for compounds **2** and **3**, and to one $[\{Cu(bpy)(H_2O)\}_2(\mu\text{-ox})]^{2+}$ complex supported on a $[SiW_{12}O_{40}]^{4-}$ POM for compound **1**. Model DFT2 corresponds to the dimers without modifications in the geometry except that water molecules replace all POM oxygen atoms in the axial positions.

where NP is the number of data points and NV is the number of variable parameters. The best-fit results are shown in Table 5. The calculated $J$ values (around $-350$ $cm^{-1}$) are in good agreement with those observed for several compounds containing $[\{Cu(bpy)\}_2(\mu\text{-ox})]^{2+}$ complexes of coplanar orbital topology,[31] which range from $-330$ to $-390$ $cm^{-1}$. Moreover, they are concordant with the DFT-calculated singlet−triplet energy gap for the coplanar $\mu$-oxalatodicopper(II) complex in $[\{Cu(tmen)(H_2O)\}_2(\mu\text{-ox})](ClO_4)_2 \cdot 1.25H_2O$.[30a] On the other hand, the calculated $g'$-factors closely reproduce the mean $g$ values deduced from the EPR spectroscopy for the $Cu^{II}$-monosubstituted Keggin POMs.

The obtained coupling constants are almost identical for compounds **2**−**4**, as was expected on the basis of the similar structural parameters of their copper−oxalate dimers, whereas that for compound **1** is slightly less antiferromagnetic. DFT calculations of the dimers at their experimental geometry have been carried out in order to determine if this difference is significant (DFT1). The models selected for compounds **2** and **3** were fragments containing two $[SiW_{12}O_{40}]^{4-}$ Keggin subunits bridged by a $[\{Cu(bpy)\}_2(\mu\text{-ox})]^{2+}$ dimer, whereas that for compound **1** consisted of one $[\{Cu(bpy)(H_2O)\}_2(\mu\text{-ox})]^{2+}$ complex supported on a $[SiW_{12}O_{40}]^{4-}$ POM. The DFT-calculated singlet−triplet energy gaps (Table 5) are significantly higher than the experimental ones, but they confirm a weaker antiferromagnetic coupling in compound **1**. In addition, they show that the $J$ values calculated for the two crystallographically independent dimers present in compound **3**, and supposedly **4**, are almost identical and very similar to that corresponding to compound **2**.

The weakening of the antiferromagnetic coupling in compound **1** with respect to compounds **2**−**4** could be attributed, in principle, to either structural or electronic factors.[30a] To check the influence of the latter, we have calculated the coupling constants for the dimers contained in compounds **1** and **3**, without modifications in the geometry except that water molecules replace all POM oxygen atoms in the axial positions (DFT2). In this case, the calculated singlet−triplet energy gaps (Table 5) are significantly lower in value than the experimental ones, but the difference of approximately 10 $cm^{-1}$ between the exchange parameters found in compounds **1** and **3** is nicely reproduced, indicating that the electronic factors do not play a significant role. Thus, the weakening of the antiferromagnetism in compound **1** should be attributed to structural factors. Taking into account that boat conformations have an almost negligible influence on the magnetic exchange, as shown by the DFT calculations reported by Cano et al.,[30a] we determined the predominant structural factor must be the 0.13 Å displacement of the Cu1 atom from its equatorial plane, which contrasts with the displacements of less than 0.06 Å that are observed in compounds **2**−**4**.

## Conclusions

The reaction between a copper-monosubstituted Keggin POM and in situ generated copper(II)−bipyridine−oxalate complexes affords a series of hybrid inorganic−metalorganic compounds, which present a dimensionality strongly dependent on the nature of the alkaline acetate/acetic acid buffer solution employed. Thus, in ammonium and rubidium buffer solutions, polymeric-hybrid-chain-containing compounds are only isolated; when the buffer solution contains potassium acetate, the compound is made up of both polymeric hybrid chains and discrete polyanions. Finally, in sodium buffer solution, a discrete hybrid compound is obtained in which the POM is sandwiched by two metalorganic complexes.

The main structural feature in these compounds is the presence of copper(II)-monosubstituted α-Keggin polyoxoanions as inorganic building blocks, on which the $\mu$-oxalatodicopper metalorganic blocks are supported. In compounds **2**−**4**, the copper−oxalate dimers act as bridging units between POMs and adopt a planar conformation, in contrast to the chair conformation afforded by DFT calculations. This flexibility can also be appreciated in compound **1**, in which the complex adopts a boat conformation. Moreover, small changes in the anchoring mode of the dicopper complex onto the polyanion affect the zigzagging angle of the $[\{SiW_{11}O_{39}Cu(H_2O)\}\{Cu_2(bpy)_2(\mu\text{-ox})\}]_n^{4n-}$ hybrid chains and, consequently, the packing and porosity.

Besides a strong antiferromagnetic coupling between copper atoms in the $[\{Cu(bpy)\}_2(ox)]^{2+}$ dimers, EPR studies show that the Keggin polyanions are able to transmit interdimeric magnetic interactions when these complexes are supported on the same $M_3O_{15}$ triad. The Keggin $Cu^{II}$ atom is involved in the exchange pathway when it is located in the remaining octahedron of this triad, whereas it appears magnetically isolated in any other POM position. This copper atom shows a low Jahn−Teller distortion due to the rigidity imposed in its coordination sphere by the pentadentate monolacunary Keggin framework.

Magnetic susceptibility studies, together with the invaluable help of DFT calculations, confirm the strong antiferromagnetic coupling in the $\mu$-oxalatodicopper complexes. The weakening of this coupling in compound **1** relative to that in compounds **2**−**4** could be attributed to structural

(31) (a) Julve, M.; Faus, J.; Verdaguer, M.; Gleizes, A. *J. Am. Chem. Soc*. **1984**, *106*, 8306. (b) Gleizes, A.; Julve, M.; Verdaguer, M.; Real, J. A.; Faus, J.; Solans, X. *J. Chem. Soc., Dalton Trans*. **1992**, 3209. (c) Castillo, O.; Muga, I.; Luque, A.; Gutiérrez-Zorrilla, J. M.; Sertucha, J.; Vitoria, P.; Román, P. *Polyhedron* **1999**, *18*, 1235. (d) Thomas, A. M.; Mandal, G. C.; Tiwary, S. K.; Rath, R. K.; Chakravarty, A. R. *J. Chem. Soc., Dalton Trans*. **2000**, 1395.

factors, and more specifically to a larger displacement of the copper ion from its equatorial plane.

**Acknowledgment.** This work was supported by Universidad del País Vasco (9/UPV 00169.310-15329/2003) and Ministerio de Ciencia y Tecnología (MAT2005-03047). S.R. thanks Gobierno Vasco for his Doctoral Fellowship. The SGI/IZO-SGIker UPV/EHU (supported by the National Program for the Promotion of Human Resources within the National Plan of Scientific Research, Development and Innovation—Fondo Social Europeo and MCyT) is gratefully acknowledged for generous allocation of computational resources.

**Supporting Information Available:** A scheme of the synthetic procedure, X-ray crystallographic files of compounds **1**−**4** in CIF format, geometric data of the $\pi$-interactions, and thermal evolution of the magnetic susceptibility for compounds **2** and **4**. This material is available free of charge via the Internet at http://pubs.acs.org.

IC051134M